


# Orthogonal-triangular decomposition ghost imaging

Jin-Fen Liu(刘进芬), Le Wang(王乐), and Sheng-Mei Zhao(赵生妹)
**Citation:**Chin. Phys. B, 2022, 31 (**8**): 084202. DOI: 10.1088/1674-1056/ac5e99
Journal homepage: http://cpb.iphy.ac.cn; http://iopscience.iop.org/cpb

**What follows is a list of articles you may be interested in**

---

## Imaging a periodic moving/state-changed object with Hadamard-based computational ghost imaging

Hui Guo(郭辉), Le Wang(王乐), and Sheng-Mei Zhao(赵生妹)
Chin. Phys. B, 2022, 31 (**8**): 084201. DOI: 10.1088/1674-1056/ac6498

## Efficient implementation of x-ray ghost imaging based on a modified compressive sensing algorithm

Haipeng Zhang(张海鹏), Ke Li(李可), Changzhe Zhao(赵昌哲), Jie Tang(汤杰), and Tiqiao Xiao(肖体乔)
Chin. Phys. B, 2022, 31 (**6**): 064202. DOI: 10.1088/1674-1056/ac48f7

## Computational ghost imaging with deep compressed sensing

Hao Zhang(张浩), Yunjie Xia(夏云杰), and Deyang Duan(段德洋)
Chin. Phys. B, 2021, 30 (**12**): 124209. DOI: 10.1088/1674-1056/ac0042

## High speed ghost imaging based on a heuristic algorithm and deep learning

Yi-Yi Huang(黄祎祎), Chen Ou-Yang(欧阳琛), Ke Fang(方可), Yu-Feng Dong(董玉峰), Jie Zhang(张杰), Li-Ming Chen(陈黎明), and Ling-An Wu(吴令安)
Chin. Phys. B, 2021, 30 (**6**): 064202. DOI: 10.1088/1674-1056/abea8c

## Handwritten digit recognition based on ghost imaging with deep learning

Xing He(何行), Sheng-Mei Zhao(赵生妹), and Le Wang(王乐)
Chin. Phys. B, 2021, 30 (**5**): 054201. DOI: 10.1088/1674-1056/abd2a5

---

# Orthogonal-triangular decomposition ghost imaging

Jin-Fen Liu(刘进芬)[1,2], Le Wang(王乐)[1], and Sheng-Mei Zhao(赵生妹)[1,3,†]

[1] *Institute of Signal Processing and Transmission, Nanjing University of Posts and Telecommunications, Nanjing* 210003, *China*
[2] *Nanjing Tech University Pujiang Institute, Nanjing* 211222, *China*
[3] *Key Laboratory of Broadband Wireless Communication and Sensor Network Technology, Ministry of Education, Nanjing* 210003, *China*

(Received 25 November 2021; revised manuscript received 11 March 2022; accepted manuscript online 17 March 2022)

Ghost imaging (GI) offers great potential with respect to conventional imaging techniques. However, there are still some obstacles for reconstructing images with high quality, especially in the case that the orthogonal measurement matrix is impossible to construct. In this paper, we propose a new scheme based on the orthogonal-triangular (QR) decomposition, named QR decomposition ghost imaging (QRGI) to reconstruct a better image with good quality. In the scheme, we can change the randomly non-orthogonal measurement matrix into orthonormal matrix by performing QR decomposition in two cases. (1) When the random measurement matrix is square, it can be firstly decomposed into an orthogonal matrix $\boldsymbol{Q}$ and an upper triangular matrix $\boldsymbol{R}$. Then let the off-diagonal values of $\boldsymbol{R}$ equal to 0.0, the diagonal elements of $\boldsymbol{R}$ equal to a constant $k$, where $k$ is the average of all values of the main diagonal, so the resulting measurement matrix can be obtained. (2) When the random measurement matrix is with full rank, we firstly compute its transpose, and followed with above QR operation. Finally, the image of the object can be reconstructed by correlating the new measurement matrix and corresponding bucket values. Both experimental and simulation results verify the feasibility of the proposed QRGI scheme. Moreover, the results also show that the proposed QRGI scheme could improve the imaging quality comparing to traditional GI (TGI) and differential GI (DGI). Besides, in comparison with the singular value decomposition ghost imaging (SVDGI), the imaging quality and the reconstruction time by using QRGI are similar to those by using SVDGI, while the computing time (the time consuming on the light patterns computation) is substantially shortened.

**Keywords:** orthogonal-triangular (QR) decomposition, ghost imaging, correlated imaging

**PACS:** 42.30.Va, 42.30.Wb **DOI:** 10.1088/1674-1056/ac5e99

## 1. Introduction

Ghost imaging (GI), also called correlated imaging, has attracted more and more attention in recent years.[1–21] The traditional GI (TGI) system consists of a signal beam and a reference beam. The signal beam, after illuminating on an object, is collected by a bucket detector without any spatial resolution. The reference beam, which never interacts with the object, is measured by a spatially resolving detector, such as a charged coupled device (CCD) or a complementary metal oxide semiconductor (CMOS) camera. By correlating the reference beam with the bucket signal, the 'ghost image' will be recovered in the reference beam. The first GI scheme was achieved based on the entangled-photon pairs, which were generated by spontaneous parametric down-conversion (SPDC).[1,2] Later, it was shown and demonstrated that GI could be realized with classical light sources, such as pseudo-thermal light,[3,4] true thermal light,[5–7] sunlight,[8] and even the screen of a television.[9] Besides, computational light patterns, produced by spatial light modulator (SLM) or digital mirror device (DMD), can also be used to realize GI. This latter approach is known as computational GI, whose light intensity detected in the reference beam is computed offline.[21]

Whereas, improving the imaging quality of GI is a key project. Recently, a variety of advanced basis illumination patterns based on ghost imaging methods have been proposed to enhance the imaging quality.[22–34] For example, Hadamard basis based ghost imaging and Fourier basis based ghost imaging,[22–31] which constitute a complete orthogonal set, can enhance the imaging quality and shorten the reconstruction time. However, if the speckle patterns are random, there is a high constant background that degrades the imaging quality. Lots of studies focus on improving the quality of the reconstructed images in the GI system with random patterns.[32–34] In 2014, peudo-inverse ghost imaging (PGI)[32] has been presented to enhance the peak signal to noise ratio (PSNR) and reduce reconstruction time for object reconstruction, by computing the pseudo-inverse of the matrix constituted by the row vectors of each speckle field. Later, singular value decomposition ghost imaging (SVDGI)[33] has been proposed to enhance the fidelity of GI by constructing a measurement matrix by using the singular value decomposition (SVD) transform. Besides, Gram–Schmidt ghost imaging[34] has been researched to enhance the efficiency of image acquisition, where a post-processing method, instead of the pre-modulation method, has been introduced to orthonormalize the patterns in a rotating ground glass scheme by using Gram–Schmidt process. Because these techniques could put the random basis patterns constitute a complete orthogonal set, so they can improve the

†Corresponding author. E-mail: zhaosm@njupt.edu.cn

© 2022 Chinese Physical Society and IOP Publishing Ltd 

quality of the reconstructed image in the GI system.

On the other hand, orthogonal-triangular (QR) decomposition technique is a genuine contribution to the field of numerical analysis, where a rectangular matrix can be decomposed into orthogonal matrix and upper triangular matrix.[35] This technique can solve the eigenvalue problem in a very satisfactory way, and reduce the time for standard eigenvalue computations to the time required for a few matrix multiplies.[36–38] Therefore, inspired by the concepts of QR decomposition technique, we propose a novel ghost imaging scheme based on QR decomposition for the case where it is impossible to obtain the orthogonal measurement matrix, named QR decomposition ghost imaging (QRGI). In general, a matrix performed by QR decomposition must satisfy one of the following conditions, and the matrix is square or with full rank. Hence, in the scheme, we construct the new measurement matrix by performing QR decomposition in two circumstances. (1) When the measurement matrix is square, it can be first decomposed into an orthogonal matrix $Q$ and an upper triangular matrix $R$. Then let the off-diagonal values of $R$ equal to 0.0, the diagonal elements of $R$ equal to a constant $k$, where $k$ is the average of all values of the main diagonal, so the resulting measurement matrix can be achieved. (2) When the measurement matrix is with full rank, then its transpose should be first computed, and followed above QR operation. Finally, we can restore the image of the object by correlating the new measurement matrix and corresponding bucket values. Numerical simulations and experiments verify the feasibility of QRGI.

The remainder of the paper is arranged as follows. QRGI is presented in Section 2. In Section 3, the performance of QRGI is discussed by numerical simulations and practical experiments. Finally, the paper is concluded by Section 4.

## 2. Theory

Figure 1 shows the schematic diagram of the proposed QRGI scheme. Here, the whole imaging process of TGI system is regarded as a series of matrix operations.[32] In the system, the series of random illumination patterns $I_1, I_2, \ldots, I_N$ are generated by a projector and then projected onto the object successively, where $N$ is the number of speckle patterns. If the transmission coefficient of each illumination pattern is a $p \times p$ matrix, the illumination pattern can be permutated into a $1 \times p^2$ row vector. Then a new measurement matrix with $N$ row vectors and $P$ column vectors can be obtained, where $P = p \times p$ is the number of pixels of the pattern. The measurement matrix is recorded as

$$\boldsymbol{A} = \begin{bmatrix} I_1(1,1) & I_1(1,2) & \cdots & I_1(p,p) \\ I_2(1,1) & I_2(1,2) & \cdots & I_2(p,p) \\ \cdots & \cdots & \cdots & \cdots \\ I_N(1,1) & I_N(1,2) & \cdots & I_N(p,p) \end{bmatrix}. \tag{1}$$

Assume that the reflective of object is a matrix $\boldsymbol{O}(x,y)$ of size $p \times p$, which can also be reshaped to a column vector of size $p^2 \times 1$ as

$$\boldsymbol{O}(x,y) = \begin{bmatrix} O(1,1) \\ O(1,2) \\ \cdots \\ O(p,p) \end{bmatrix}. \tag{2}$$

Likewise, the $N$ bucket values measured by a bucket detector can be permutated into a $N \times 1$ column vector. Mathematically speaking, it must have the following linear relationship:

$$\begin{bmatrix} B_1 \\ B_2 \\ \cdots \\ B_N \end{bmatrix} = \boldsymbol{A} \begin{bmatrix} O(1,1) \\ O(1,2) \\ \cdots \\ O(p,p) \end{bmatrix}. \tag{3}$$

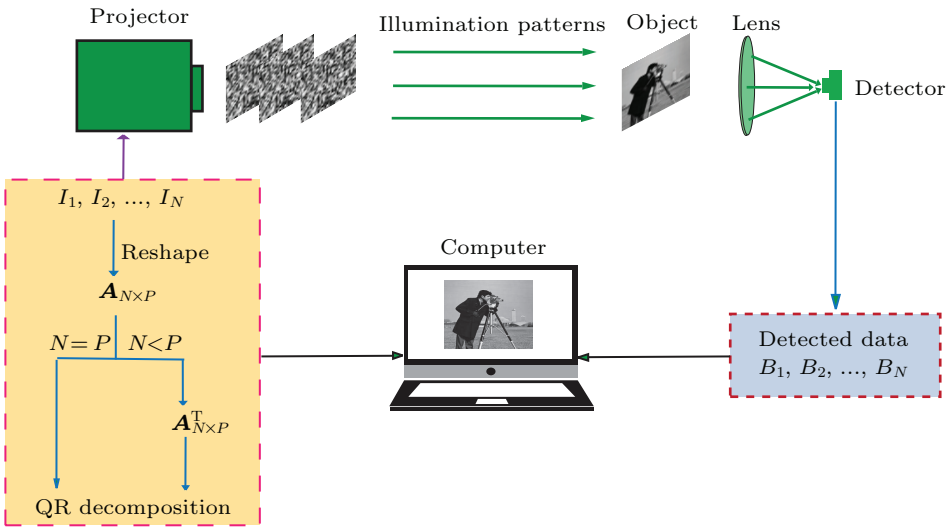



**Fig. 1.** A schematic diagram of the QRGI scheme.

Hence, according to the second-order correlation (2C) algorithm,[39] the estimation of $\boldsymbol{O}(x,y)$ can be obtained by

$$\hat{\boldsymbol{O}}_{\mathrm{GI}}(x,y)=\frac{1}{N}\sum_{i=1}^{N}(B_i-\langle B_i\rangle)I_i(x,y), \tag{4}$$

where the symbol $\sum_{i=1}^{N}$ calculates the summation of first $N$ terms, $\langle\cdot\rangle$ calculates the average value of a vector, and $B_i=\iint I_i(x,y)O(x,y)\,\mathrm{d}x\mathrm{d}y$.

We can rewrite Eq. (4) as the matrix formula, which is expressed as

$$\begin{aligned}\hat{\boldsymbol{O}}_{\mathrm{GI}}(x,y)=&\frac{1}{N}\begin{bmatrix}I_1(1,1) & I_2(1,1) & \cdots & I_N(1,1)\\ I_1(1,2) & I_2(1,2) & \cdots & I_N(1,2)\\ \cdots & \cdots & \cdots & \cdots\\ I_1(p,p) & I_2(p,p) & \cdots & I_N(p,p)\end{bmatrix}\begin{bmatrix}B_1\\ B_2\\ \cdots\\ B_N\end{bmatrix}\\ &-\langle B\rangle\begin{bmatrix}\langle I(1,1)\rangle\\ \langle I(1,2)\rangle\\ \cdots\\ \langle I(p,p)\rangle\end{bmatrix}.\end{aligned} \tag{5}$$

Extracting the first term on the right hand of Eq. (5) and substituting Eqs. (1)–(3) into it, we can get[33]

$$\hat{\boldsymbol{O}}_{\mathrm{GI}}(x,y)=\frac{1}{N}\boldsymbol{A}^{\mathrm{T}}\boldsymbol{A}\boldsymbol{O}(x,y), \tag{6}$$

where $\boldsymbol{A}^{\mathrm{T}}$ refers to the transposition operation on $\boldsymbol{A}$. Apparently, only when $\boldsymbol{A}^{\mathrm{T}}\boldsymbol{A}$ is close to unit matrix, the image of the object can be perfectly restored. When $\boldsymbol{A}$ is an orthogonal matrix, the object will be quickly and exactly reconstructed.

Hence, we introduce the QR decomposition technique into GI system. Importantly, the measurement matrix must satisfy one of the following conditions, and the matrix is square or with full rank. Therefore, we demonstrate QRGI scheme as follows.

**(1) Matrix $\boldsymbol{A}$ is a square matrix** ($N=P$)

At first, we discuss the situation when the number of measurements is equal to the number of pixels of the image, i.e., $N=P$. After taking QR decomposition, matrix $\boldsymbol{A}$ can be decomposed into two products

$$\boldsymbol{A}=\boldsymbol{Q}\times\boldsymbol{R}, \tag{7}$$

where $\boldsymbol{Q}$ is $(N\times P)$ orthogonal and $\boldsymbol{R}$ is $(P\times P)$ upper triangular.

Substituting Eq. (7) into Eq. (6), we can get

$$\begin{aligned}\hat{\boldsymbol{O}}_{\mathrm{QRGI}}(x,y)&=\frac{1}{N}(\boldsymbol{Q}\boldsymbol{R})^{\mathrm{T}}(\boldsymbol{Q}\boldsymbol{R})\boldsymbol{O}(x,y)\\&=\frac{1}{N}\boldsymbol{R}^{\mathrm{T}}\boldsymbol{Q}^{\mathrm{T}}\boldsymbol{Q}\boldsymbol{R}\boldsymbol{O}(x,y)\\&=\frac{1}{N}\boldsymbol{R}^{\mathrm{T}}\boldsymbol{R}\boldsymbol{O}(x,y),\end{aligned} \tag{8}$$

where $\boldsymbol{R}^{\mathrm{T}}\boldsymbol{R}$ is still an upper triangular matrix. Its diagonal elements represent the effective information for reconstruction. Therefore, we set the off-diagonal values of $\boldsymbol{R}$ equal to 0.0, the diagonal elements of $\boldsymbol{R}$ equal to a constant $k$, where $k$ is the average of all values of the main diagonal, and $\boldsymbol{R}^{\mathrm{T}}\boldsymbol{R}$ in Eq. (8) can be replaced by $k^2\boldsymbol{E}$, where $\boldsymbol{E}$ refers to an unit matrix. Hence, Eq. (8) can be approximate to

$$\begin{aligned}\hat{\boldsymbol{O}}_{\mathrm{QRGI}}(x,y)&\approx\frac{1}{N}(k\boldsymbol{E})^{\mathrm{T}}(k\boldsymbol{E})\boldsymbol{O}(x,y)\\&=\frac{k^2}{N}\boldsymbol{E}^{\mathrm{T}}\boldsymbol{E}\boldsymbol{O}(x,y)\\&=\frac{k^2}{N}\boldsymbol{O}(x,y).\end{aligned} \tag{9}$$

Obviously, according to Eq. (9), the image of the object can be perfectly reconstructed.

**(2) Matrix $\boldsymbol{A}$ is a full rank matrix** ($N<P$)

Taking less number of measurements to reconstruct the object is the key problem in the GI system. In general, the illumination patterns generated by the projector are random and independent, so $\boldsymbol{A}^{\mathrm{T}}$ is with full rank, and $\mathrm{rank}(\boldsymbol{A})=N$. Thus, taking QR decomposition on $\boldsymbol{A}^{\mathrm{T}}$ of size $P\times N$, we can obtain

$$\boldsymbol{A}^{\mathrm{T}}=\boldsymbol{Q}\times\boldsymbol{R}, \tag{10}$$

where $\boldsymbol{Q}$ is $P\times N$ orthogonal, and $\boldsymbol{R}$ is $N\times N$ upper triangular. Substituting Eq. (10) into Eq. (6), we can get

$$\begin{aligned}\hat{\boldsymbol{O}}_{\mathrm{QRGI}}(x,y)&=\frac{1}{N}(\boldsymbol{Q}\boldsymbol{R})(\boldsymbol{Q}\boldsymbol{R})^{\mathrm{T}}\boldsymbol{O}(x,y)\\&=\frac{1}{N}\boldsymbol{Q}\boldsymbol{R}\boldsymbol{R}^{\mathrm{T}}\boldsymbol{Q}^{\mathrm{T}}\boldsymbol{O}(x,y).\end{aligned} \tag{11}$$

Similarly, $\boldsymbol{R}=k\boldsymbol{E}$, then Eq. (11) can be simplified as

$$\begin{aligned}\hat{\boldsymbol{O}}_{\mathrm{QRGI}}(x,y)&=\frac{1}{N}\boldsymbol{Q}(k\boldsymbol{E})(k\boldsymbol{E})^{\mathrm{T}}\boldsymbol{Q}^{\mathrm{T}}\boldsymbol{O}(x,y)\\&=\frac{k^2}{N}\boldsymbol{Q}\boldsymbol{E}\boldsymbol{E}^{\mathrm{T}}\boldsymbol{Q}^{\mathrm{T}}\boldsymbol{O}(x,y)\\&=\frac{k^2}{N}\boldsymbol{Q}\boldsymbol{Q}^{\mathrm{T}}\boldsymbol{O}(x,y).\end{aligned} \tag{12}$$

From Eq. (12) we can see that the closer the $\boldsymbol{Q}\boldsymbol{Q}^{\mathrm{T}}$ is to unit matrix, the higher the quality of the reconstructed image is. Therefore, it is in principle that QRGI can get a restored image with a higher fidelity. Noted that the case of $N>P$ is not considered since we have restored the object perfectly when $N=P$.

## 3. Results and discussion

In this section, we will verify the proposed QRGI scheme by both numerical simulations and experiments. In order to demonstrate the quality of the reconstructed image, mean square error (MSE) is used as an objective evaluation,[40] which is defined as

$$\mathrm{MSE}=\frac{1}{P}\sum_{x,y}(\hat{\boldsymbol{O}}(x,y)-\boldsymbol{O}(x,y))^2, \tag{13}$$

where $\boldsymbol{O}(x,y)$ and $\hat{\boldsymbol{O}}(x,y)$ refer to the original and the reconstructed object respectively, $(x,y)$ is Cartesian coordinate, and $P$ is the number of pixels of the image.

The experimental setup is shown in Fig. 2, which includes a projector (DLP LightCrafter 4500), a photodetector (Thorlabs PMM02-1), a data acquisition card (National Instrument USB-6341), and a computer (Intel(R) Core(TM) i3-8145U CPU @ 2.10 GHz; RAM: 8.00 GB). As the bit depth of the projector is limited to 8, the quantization noise is introduced when the values of the random pattern are quantized. The speckle patterns, generated by the projector, are projected onto the target object. The photodetector, placed at the opposite of the object, is used to detect the light intensity reflecting from the object, and the data acquisition card (DAQ) is adopted to perform analogue-to-digital convert. Finally, the computer can reconstruct the object by correlating the speckle patterns and corresponding bucket values.

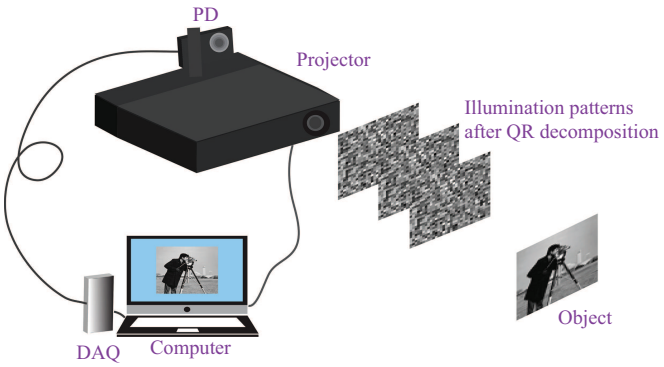



**Fig. 2.** A schematic diagram of the QRGI scheme experimental system. PD: photodetector. DAQ: data acquisition card.

At first, we compute and display the products of $\boldsymbol{A}^{\mathrm{T}}\boldsymbol{A}$ and $\boldsymbol{A}_{\mathrm{QR}}^{\mathrm{T}}\boldsymbol{A}_{\mathrm{QR}}$ to reflect which one is closer to unit matrix. We use a random $\boldsymbol{A}$ of size $64\times64$ pixels, then construct $\boldsymbol{A}_{\mathrm{QR}}$ by our method. Later, we normalize the values of $\boldsymbol{A}^{\mathrm{T}}\boldsymbol{A}$ and $\boldsymbol{A}_{\mathrm{QR}}^{\mathrm{T}}\boldsymbol{A}_{\mathrm{QR}}$ into 0–255 grayscale, and graphically display them in Fig. 3, where the insets are the 2D grayscale images of the matrixes, and $x$ and $y$ represent the row and column coordinates of their elements, respectively. From the 2D matrix of Figs. 3(a) and 3(b), we can see that $\boldsymbol{A}_{\mathrm{QR}}^{\mathrm{T}}\boldsymbol{A}_{\mathrm{QR}}$ is closer to unit matrix than $\boldsymbol{A}^{\mathrm{T}}\boldsymbol{A}$ since the off-diagonal values of $\boldsymbol{A}^{\mathrm{T}}\boldsymbol{A}$ are much larger than those in $\boldsymbol{A}_{\mathrm{QR}}^{\mathrm{T}}\boldsymbol{A}_{\mathrm{QR}}$. Besides, from the 3D maps of Figs. 3(a) and 3(b), we can see that $\boldsymbol{A}^{\mathrm{T}}\boldsymbol{A}$ fluctuates violently, the diagonal elements are submerged by the off-diagonal values of $\boldsymbol{A}^{\mathrm{T}}\boldsymbol{A}$, while the off-diagonal values in $\boldsymbol{A}_{\mathrm{QR}}^{\mathrm{T}}\boldsymbol{A}_{\mathrm{QR}}$ are much clear, this also demonstrates that $\boldsymbol{A}_{\mathrm{QR}}^{\mathrm{T}}\boldsymbol{A}_{\mathrm{QR}}$ is closer to unit matrix than $\boldsymbol{A}^{\mathrm{T}}\boldsymbol{A}$. Thus, QRGI is theoretically feasible.

Next, we testify the validity of QRGI by numerical simulations and experiments. In accordance with the experimental condition, we normalize the values of random speckle patterns into 0–255 grayscale in simulations, which will introduce the quantization noise. Choosing two pictures as the original objects, one is a grayscale image ('Cameraman') and the other one is a binary image ('Star'). The results are shown in Fig. 4, where Fig. 4(a) are original images, Fig. 4(b) shows the reconstructed images with the size of $32\times32$ pixels, where the number of measurements $N=1024$, and Fig. 4(c) displays the reconstructed results with the size of $64\times64$ pixels, where the number of measurements $N=4096$. The first two rows are simulated results, from which we can see that taking the Nyquist limit measurements (equal to the number of the image pixels), QRGI can perfectly reconstruct the object, while the images restored by TGI and DGI are more or less polluted by noise. Besides, taking the grayscale 'Cameraman' of $64\times64$ pixels for instance, there are two order of magnitude improvement in MSEs values in comparison with those of TGI and DGI. The last two experimental results also show that QRGI has a better performance than that of TGI and DGI. For both binary and grayscale objects, the imaging quality of the reconstructed images of QRGI scheme is better than that of TGI and DGI and corresponding MSEs are smaller, which shows that the proposed QRGI scheme has a better reconstruction performance.

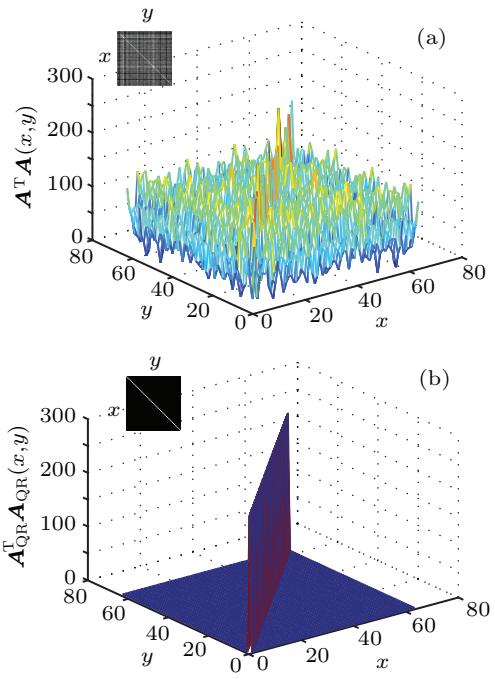



**Fig. 3.** Comparison of $\boldsymbol{A}^{\mathrm{T}}\boldsymbol{A}$ and $\boldsymbol{A}_{\mathrm{QR}}^{\mathrm{T}}\boldsymbol{A}_{\mathrm{QR}}$. (a) $\boldsymbol{A}^{\mathrm{T}}\boldsymbol{A}$, (b) $\boldsymbol{A}_{\mathrm{QR}}^{\mathrm{T}}\boldsymbol{A}_{\mathrm{QR}}$. Here $x$: row coordinates of the matrix; $y$: column coordinates of the matrix.

Figure 5 shows the MSEs curve against the different numbers of measurements by using TGI, DGI and QRGI schemes. Here the object is a binary 'Star' image with the size of $64\times64$ pixels, where Fig. 5(a) shows the simulated results, and Fig. 5(b) shows the experimental results. The results indicate that as the number of measurements increases, the MSEs values decrease gradually for three methods, while the proposed QRGI scheme has a more rapidly rate. Compared with TGI and DGI, QRGI scheme could achieve better imaging quality at the same number of measurements.

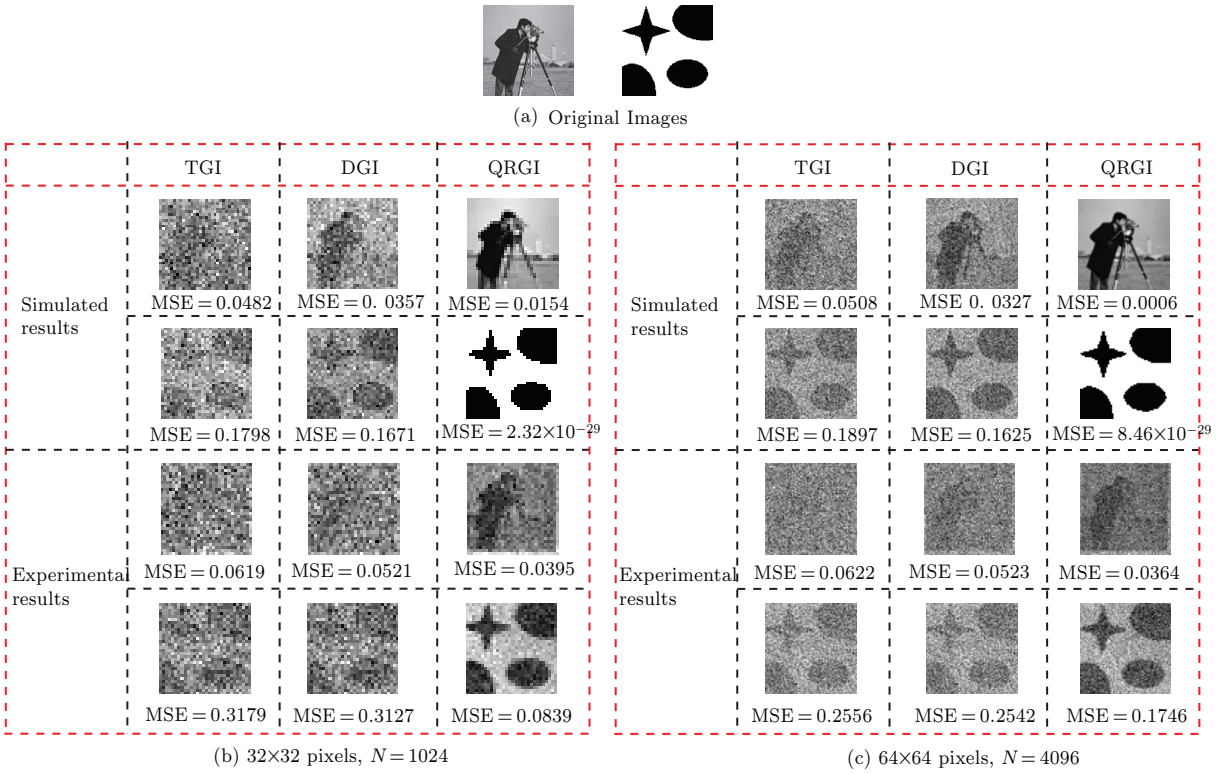



**Fig. 4.** Simulated and experimental results comparison. (a) Original objects. (b) $32 \times 32$ pixels, and $N = 1024$. (c) $64 \times 64$ pixels, and $N = 4096$.

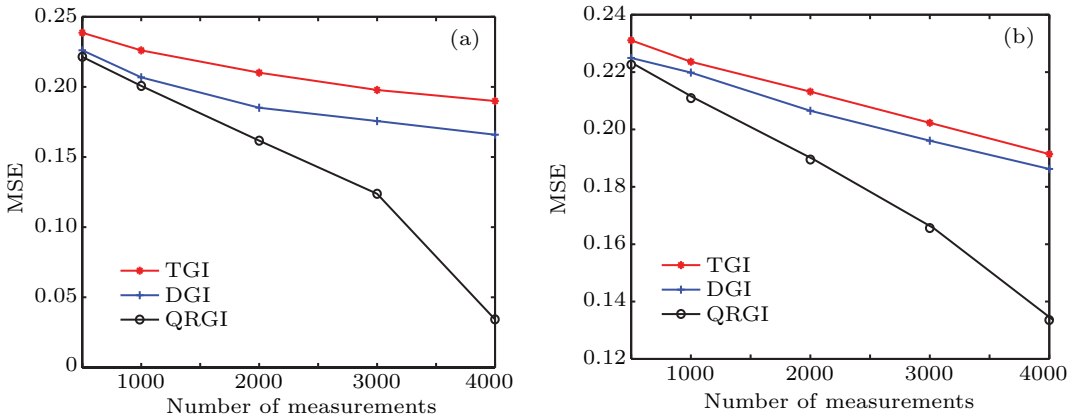



**Fig. 5.** The MSEs curve against the different numbers of measurements by TGI, DGI and QRGI. (a) The simulated results. (b) The experimental results.

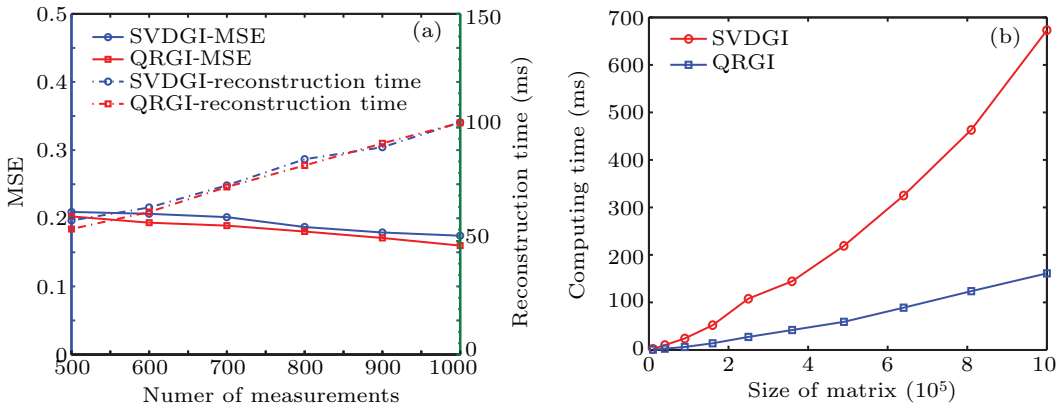



**Fig. 6.** Comparison by using QRGI scheme and SVDGI scheme. (a) The MSEs and reconstruction time curve against different numbers of measurements by using QRGI and SVDGI from experimental results. (b) The computing time curve against the size of the measurement matrix by using SVDGI and QRGI from simulated results.

Figure 6 further shows the MSEs and reconstruction time curve against different numbers of measurements by using QRGI and SVDGI from experimental results, together with the computing time (the time-consuming on the light patterns computation) curve against different numbers of measurements by QRGI and SVDGI from simulated results. Here, a binary 'Star' image with the size of $32 \times 32$ pixels is selected as the object in Fig. 6(a). The results show that the performance of QRGI and SVDGI are almost the same. Their MSEs values and reconstruction time are very closer at the same number of measurements, which indicates that QRGI can match the performance of SVDGI. Besides, a random rectangle matrix is selected as the measurement matrix to do QR decomposition and SVD transform in Fig. 6(b), from which we can see that with the increase of the size of the matrix, both schemes has a longer computing time, but the proposed scheme costs a less computing time. Therefore, the proposed QRGI scheme has a promising prospect in real applications.

## 4. Conclusion

In the paper, we have proposed a novel GI scheme to get a better imaging performance with QR decomposition, named QR decomposition ghost imaging, where the whole imaging process of GI system is regarded as a series of matrix operations. The numerical simulations and experimental results have shown that the reconstructed images by using QRGI have a better performance than those reconstructed by using TGI and DGI, and this improvement of imaging quality is without the consumption of physical dimensions of light field. In addition, the proposed QRGI scheme can match the performance of SVDGI, while the proposed QRGI scheme requires a shorter computing time. The proposed scheme is appropriate for the cases where it is impossible to obtain the orthogonal measurement matrix. We believe that the usage of QR decomposition developed in the field of numerical analysis to the GI system provides a way for new GI schemes.

## Acknowledgements

Project supported by the National Natural Science Foundation of China (Grant Nos. 61871234 and 62001249), the Postgraduate Research & Practice Innovation Program of Jiangsu Province, China (Grant No. KYCX20_0729), Natural Science Research Project of Higher Education of Jiangsu Province, China (Grant No. 20KJB510030), and Research project of NanJing Tech University Pujiang Institute (Grant No. njpj2020-1-02).

## References

[1] Pittman T B, Shih Y H, Strekalov D V and Sergienko A V 1995 *Phys. Rev. A* **52**R3429(R)
[2] Strekalov D V, Sergienko A V, Klyshko D N and Shih Y H 1995 *Phys. Rev. Lett.* **74** 3600
[3] Ferri F, Magatti D, Gatti A, Bache M, Brambilla E and Lugiato L A 2005 *Phys. Rev. Lett.* **94** 183602
[4] Ferri F, Magatti D, Lugiato L A and Gatti A 2010 *Phys. Rev. Lett.* **104** 253603
[5] Zhang D, Zhai Y H, Wu L A and Chen X H 2005 *Opt. Lett.* **30** 2354
[6] Chen X H, Liu Q, Luo K H and Wu L A 2009 *Opt. Lett.* **34** 695
[7] Cao D Z, Li Q C, Zhuang X C, Ren C, Zhang S H and Song X B 2018 *Chin. Phys. B* **27** 123401
[8] Liu X F, Chen X H, Yao X R, Yu W K, Zhai G J and Wu L A 2014 *Opt. Lett.* **39** 2314
[9] Zhang X, Yin H, Li R, Hong J, Ai S, Zhang W, Wang C, Hsieh J, Li Q and Xue P 2020 *Opt. Exp.* **28** 17232
[10] Zhang Y D and Zhao S M 2016 *Chin. Phys. B* **26** 054205
[11] Zhao S, Wang L, Liang W, Cheng W and Gong L 2015 *Opt. Commun.* **353** 90
[12] Yin M Q, Wang L and Zhao S M 2019 *Chin. Phys. B* **28** 094201
[13] Yin X L, Xia Y J and Duan D Y 2018 *Opt. Exp.* **26** 18944
[14] Cao D Z, Xu B L, Zhang S H and Wang K G 2015 *Chin. Phys. Lett.* **32** 114208
[15] Li H X, Bai Y F, Shi X H, Nan S Q, Qu L J, Shen Q and Fu X Q 2017 *Chin. Phys. B* **26** 104204
[16] Chen L, Yan D, Song L J and Zhang T 2019 *Chin. Phys. Lett.* **36** 030302
[17] Chen W and Chen X 2015 *Opt. Lasers. Eng.* **73** 123
[18] Zhang H and Duan D 2021 *Chin. Opt. Lett.* **19** 101101
[19] Zhou Y, Guo S X, Zhong F and Zhang T 2019 *Chin. Phys. B* **28** 084204
[20] Si Y, Kong L J, Li Y N, Tu C H and Wang H T 2016 *Chin. Phys. Lett.* **33** 034203
[21] Shapiro J H 2008 *Phys. Rev. A* **78** 061802(R)
[22] Wang L and Zhao S 2016 *Photon. Res.* **4** 240
[23] Liu J, Wang L and Zhao S 2021 *Opt. Exp.* **29** 41485
[24] Wang L and Zhao S 2020 *IEEE. Photon. J.* **12** 6901113
[25] Sun M J, Meng L T, Edgar M P, Padgett M J and Radwell N 2017 *Sci. Rep.* **7** 3464
[26] Zhang Z, Wang X, Zheng G and Zhong J 2017 *Opt. Exp.* **25** 19619
[27] Zhang C, Gong W and Han S 2013 *Appl. Phys. Lett.* **102** 021111
[28] Liu B L, Yang Z H, Liu X and Wu L A 2017 *J. Mod. Opt.* **64** 259
[29] Yu W K, Yao X R, Liu X F, Lan R M, Wu L A, Zhai G J and Zhao Q 2016 *Opt. Commun.* **371** 105
[30] Zhou C, Huang H Y, Liu B and Song L J 2016 *Acta Opt. Sin.* **36** 0911001
[31] Xiao Y, Zhou L N and Chen W 2019 *IEEE Photon. J.* **11** 7800411
[32] Zhang C, Guo S X, Cao J S, Guan J and Gao F L 2014 *Opt. Exp.* **22** 30063
[33] Zhang X, Meng X, Yang X, Wang Y, Yin Y, Li X, Peng X, He W, Dong G and Chen H 2018 *Opt. Exp.* **26** 12948
[34] Luo B, Yin P Q, Yin L F, Wu G H and Guo H 2018 *Opt. Exp.* **26** 23093
[35] Gander W 1980 *Algorithms for the QR-Decomposition* (Research Report 80-02 Angewandte Mathematik ETH) pp. 1–27
[36] Francis J G F 1961 *Comput. J.* **4** 265
[37] Sharma A, Paliwal K K, Imoto S and Miyano S 2013 *Int. J. Mach. Learn. and Cyber.* **4** 679
[38] Parlett B N 2000 *Comput. Sci. Eng.* **2** 38
[39] Wang L and Zhao S 2020 *Chin. Phys. B* **29** 024204
[40] Wang L and Zhao S 2021 *Opt. Exp.* **29** 24486